Biochemistry and Biophysics Reports 42 (2025) 102003

Contents lists available at ScienceDirect

Biochemistry and Biophysics Reports

journal homepage: www.elsevier.com/locate/bbrep

Clinical data investigation identifies MARK3 as an oncogenic driver in castration-resistant prostate cancer

Rajnikant Raut [a], Devesh Srivastava [a], Vinayak Nayak [a], Taruna Saini [a], Parth Gupta [a], Amit Kumar Chakraborty [b], Chumki Choudhury [b], Manish V. Bais [b], Parul Mishra [c], Ashish Misra [a,*]

[a] Department of Biotechnology, Indian Institute of Technology Hyderabad, Kandi, Sangareddy, 502285, India
[b] Department of Translational Dental Medicine, Boston University Henry M. Goldman School of Dental Medicine, 700 Albany Street, Boston, MA, 02118, USA
[c] Department of Animal Biology, School of Life Sciences, University of Hyderabad, Hyderabad, 500046, India

ARTICLE INFO

Keywords:
Cancer
CRPC
Prostate cancer
PCC0208017
22Rv1
MARK3

ABSTRACT

Castration-resistant prostate cancer (CRPC) represents an aggressive and fatal form of prostate cancer that emerges following resistance to androgen deprivation therapy. Despite the availability of various drugs that can enhance the quality and prolong the survival of CRPC patients, resistance to these therapies is frequently observed, making the disease increasingly difficult to treat. Altered expression of kinases and phosphatases is a critical driver of CRPC and presents a potential target for more effective treatments. In this study, we have performed comprehensive transcriptomic analysis of ~359 normal and CRPC patient samples from The Cancer Genome Atlas to identify the differentially expressed kinases and phosphatases in patient samples. We shortlisted the candidate genes based on their differential expression profiles, associations with patient survival, Gleason scores, and their impact on the fitness of prostate cancer cell lines. Our in-silico analysis identified microtubule affinity-regulating kinase 3 (MARK3) as a novel CRPC driver that is upregulated in CRPC patients, linked with poor survival outcomes, and affects the fitness of CRPC cells. Furthermore, we found that pharmacological inhibition of MARK3 using PCC0208017, a MARK3 inhibitor, leads to reduced cell viability, migration potential, and cell cycle arrest in the G1 phase in prostate cancer cells. Additionally, RNA sequencing analysis in 22Rv1 cells treated with the MARK3 inhibitor revealed that MARK3 influences genes involved in androgen response, epithelial-mesenchymal transition, mTOR, and myc-signalling, underscoring its pivotal role in CRPC progression. Taken together, our results establish MARK3 as a novel and promising therapeutic target in CRPC.

1. Introduction

Prostate cancer (PCa) is an age-dependent malignancy of prostate tissue and the second most commonly occurring cancer in males worldwide. Primary treatment involves anti-hormone therapy to decrease or block the action of androgens. This therapy can be given either alone or in combination with radiation and/or chemotherapy to enhance its effectiveness in high-risk patients [1,2]. Despite the promise, nearly 20 % of PCa patients receiving androgen deprivation therapy develop castration-resistant prostate cancer (CRPC), which is an aggressive form of PCa associated with a poor survival rate [3]. Approximately, one-third of CRPC patients transition from a non-metastatic to metastatic form of this cancer within the initial two years of diagnosis and treatment, further complicating the disease prognosis [4]. Chemotherapy with a combination of apalutamide and enzalutamide or abiraterone has shown therapeutic promise in metastatic CRPC (mCRPC), but the treatment leads to numerous side effects [5–8]. Although these current approaches have acceptable clinical benefits, the complexity of disease manifestation and poor life expectancy continuously stresses upon the urgency to develop effective and more advanced therapeutic strategies to treat this cancer.

Recurrent genetic alterations revealed by large scale genome and exome sequencing underlies both primary and metastatic CRPC. These genetic modifications include either point mutations or large chromosomal aberrations that impact the normal prostate development, cell cycle regulation, androgen synthesis and signalling [9]. At the molecular level, these genetic changes often impact gene expression and modification of key substrates involved in the onset and progression of CRPC.

* Corresponding author.
E-mail address: ashishmisra@bt.iith.ac.in (A. Misra).

https://doi.org/10.1016/j.bbrep.2025.102003
Received 8 November 2024; Received in revised form 4 March 2025; Accepted 1 April 2025

For example, many proteins of the phosphoinositide 3-kinase (PI3K) and mitogen-activated protein kinase (MAPK) signalling pathway are shown to be aberrantly phosphorylated to trigger cell proliferation and metastasis in CRPC [9]. Although the downstream targets of some mis-regulated kinases and phosphatases in CRPC are known, the clinical significance of newly identified cancer drivers is still emerging. Recent study using microarray analysis of prostatectomy samples from high-risk cancer patients showed the elevated expression of DNA-dependent protein kinase (*DNAPK*) that modulates Wnt-signaling and metastasis in PCa [10]. Other large scale studies have highlighted the role of RAF family, MERTK, and NTRK2 in bone and visceral metastasis of PCa [11] as well as the role of MAPK8IP3, a JNK pathway kinase, in PCa and CRPC progression [12]. Moreover, Src family kinases (SFK) are also associated with the PCa and numerous SFK inhibitors are currently under the different stages of clinical trials [13].

Potential predictors of PCa have been identified from multi-omics analysis of patient samples but identification of putative CRPC markers is still limited. Aberrant activity of some phosphatases is known to be associated with poor CRPC disease outcomes [14,15] and a deeper analysis of the clinical data is required to identify novel candidates with substantial druggability potential. In this study, we have comprehensively investigated ~359 normal and CRPC patient samples obtained from the cancer genome atlas (TCGA) to identify clinically relevant kinases and phosphatases. We analysed the differential gene expression (DGE) profile within the cohort and subjected the differentially expressed kinases and phosphatases in these samples to Kaplan-Meier survival estimation. Candidates associated with poor survival outcomes were considered for the downstream analyses. We performed their co-occurrence analysis with highly upregulated genes in CRPC identified from our overall differential expression and DepMap-based fitness dependency analysis. We identified microtubule affinity regulating kinase 3 (MARK3) as a potential novel driver of CRPC and observed that pharmacological inhibition of MARK3 with PCC0208017 (known inhibitor of MARK3) reduced cell survival, wound healing ability, and cell cycle arrest in 22Rv1 and PC3 cell lines. RNA sequencing in 22Rv1 cells upon PCC0208017 treatment demonstrated that MARK3 inhibition greatly reduces the expression of androgen receptor variant 7 (AR-V7) downstream target genes that are critical drivers of CRPC. The hallmark analysis of 22Rv1 RNA-Seq data revealed a significant negative enrichment of androgen response, epithelial-mesenchymal transition, mTORC1, and myc signalling gene sets upon PCC0208017 inhibition. Overall, with the comprehensive patient data analysis and experimental validations, we highlight the importance of MARK3 in the CRPC progression.

2. Methodology

2.1. Differential expression analysis

Raw expression data from prad_su2c_2019 study (n = 208) [16] & WCDT-MCRPC study (n = 99) [17] of CRPC patient samples was obtained using Bioconductor package TCGAbiolinks [18] in R studio [19]. Primary prostate patient samples (n = 498) and normal prostate samples (n = 52) were also obtained from the TCGA-GDC portal (Project Id: TCGA-PRAD). Differential gene expression analysis was performed considering normal prostate samples as a control group and patient samples as the experimental group in R studio using *limma* pipeline, an inbuilt function of TCGAbiolinks package.

We obtained the list of human kinases from KinMap, an online tool for kinome data [20], and list of phosphatases was obtained from the literature. We extracted the kinase and phosphatase expression data from overall gene expression data using a subset function in R studio and generated a volcano plot for overall gene expression as well as for kinase gene expression using R package EnhancedVolcano [21]. Heatmaps were generated in Rstudio using the Bioconductor package ComplexHeatmap [22] combined with Circlize [23].

2.2. Kaplan-Meier survival estimates and expression plots

Patient data from the prad_su2c_2019 study was considered for survival analysis. We performed Kaplan-Meier survival estimates for all the dysregulated kinases and phosphatases by grouping patients with positive and negative z-scores. The positive z-score group represents patients with higher expression of a particular gene, and the negative z-score group represents a lower expression of a specific gene. This analysis was performed with the inbuilt function in cbioportal. The KM plots were generated with GraphPad PRISM software.

2.3. Co-occurrence and fitness dependency analysis

We performed co-occurrence analysis in cbioportal for kinase and phosphatases associated with poor survival (KPPS) with top differentially expressed genes (DEGs) associated with growth and development. DEGs with $|\log_2 FC > 3|$ were filtered and the list was submitted to the Search Tool for the Retrieval of Interacting Genes/Proteins (STRING) [24] database and obtained Reactome pathway data. For co-occurrence analysis, we selected the candidates that belong to the pathways associated with growth and development. We performed the analysis in cbioportal, and to enhance the sensitivity of our analysis, we considered co-occurrence events with |p-value <0.05| as significant. Next, we generated the heatmap for these selected events with R package ggplot2 [25].

The fitness score of each KPPS across prostate cancer cell lines was obtained from the Dependency Map (DepMap) portal [26]. The fitness data was visualized in a heatmap plotted with the *ComplexHeatmap* package.

2.4. Cell viability assay

Both 22Rv1 and PC3 cell lines were obtained from ATCC and cultured in RPMI-1640 medium (ATCC) supplemented with 10 % fetal bovine serum and 1 % penicillin-streptomycin cocktail. Cells were cultured in a 10 cm Petri dish and sub-cultured for further use. These sub-cultured cells were then counted with a hemocytometer and approximately 10,000 cells were seeded in a 12-well plate. Cells were allowed to reach 40 % confluency and then treated with 0 nM, 1 nM, 10 nM, 100 nM, & 300 nM of PCC0208017 (MedChemExpress). Inhibitor stocks were prepared in DMSO as per manufacturer instructions.

For the assay, cells were treated for a total of 72 h, and images were captured at various time points (24 h, 48 h, & 72 h). Before imaging, cells were treated with the NucBlue™ (Thermo-Fisher Scientific), a dye that stains live cell nucleus. Imaging was performed 20X with Keyence fluorescence microscope. Live cells in each well were counted with the inbuilt function of Keyence software, and the corresponding IC50 analysis and plotting were performed in GraphPad PRISM software.

2.5. Wound healing assay

For this assay, ~10^5 cells (both 22Rv1 and PC3) were seeded in a 12-well plate. Cells were allowed to attach evenly and reach maximum confluency. Afterwards, a scratch was added in a straight line with p200 pipette tip in each well and treated with 0 nM, 10 nM, 50 nM, and 100 nM of PCC0208017 in a triplicate. Imaging was performed at 0 h, 48 h, and 72 h for 22Rv1 and 0 h and 24 h for PC3 to monitor the wound healing. Quantification was performed with the ImageJ software and barplots were generated using GraphPad PRISM.

2.6. Cell cycle analysis

To perform the analysis, ~1x10^5 cells were seeded in a 6-well plate and incubated for 48 h. Cells were then treated with varying concentration of PCC0208017 (0 nM, 10 nM, 50 nM, and 100 nM) and incubated for another 24 h. After incubation, cells were trypsinized and

harvested in 15 mL tubes. Next, they were subjected to 1X PBS wash and fixed with 70 % ethanol following which they were incubated for 30 min on ice and overnight incubation at 4 °C. Staining was performed with 500ul of 50 μg/mL propidium iodide along with the 100 μg/mL RNase A, and allowed to incubate at 37 °C for 40 min. Since propidium iodide is light sensitive, we performed this experiment in a controlled dark conditions. Upon successful staining, cells were subjected to the flow cytometry with a five-laser 64-color Cytek Aurora spectral flow cytometer and the data was analysed with FCS Express software.

2.7. RNA sequencing and analysis

We extracted total RNA from 22Rv1 cells treated with DMSO (control) or MARK3 inhibitor using TRIzol (n = 4/condition). mRNA was purified from total RNA using poly-T oligo-attached magnetic beads and ~400 ng of RNA was sent for paired-end RNA sequencing. We obtained around 20 million clean reads per sample. Raw FASTQ sequencing reads were subjected to quality control and preprocessing with in-house Perl script of Novogene before aligning to the reference genome. Filtered data was mapped against the reference genome of *Homo sapiens* (hg38) with total mapping percent ranging from 85 % to 89 %. FeatureCounts (v1.5.0-p3) was used to count the reads numbers mapped to each gene. Subsequently, DGE analysis was performed using the *DESeq2* package in R/Bioconductor. Volcano plots for DEGs were generated using *EnhancedVolcano* package in R. Hallmark analysis was performed with gene set enrichment analysis (GSEA-v4.3.2) tool.

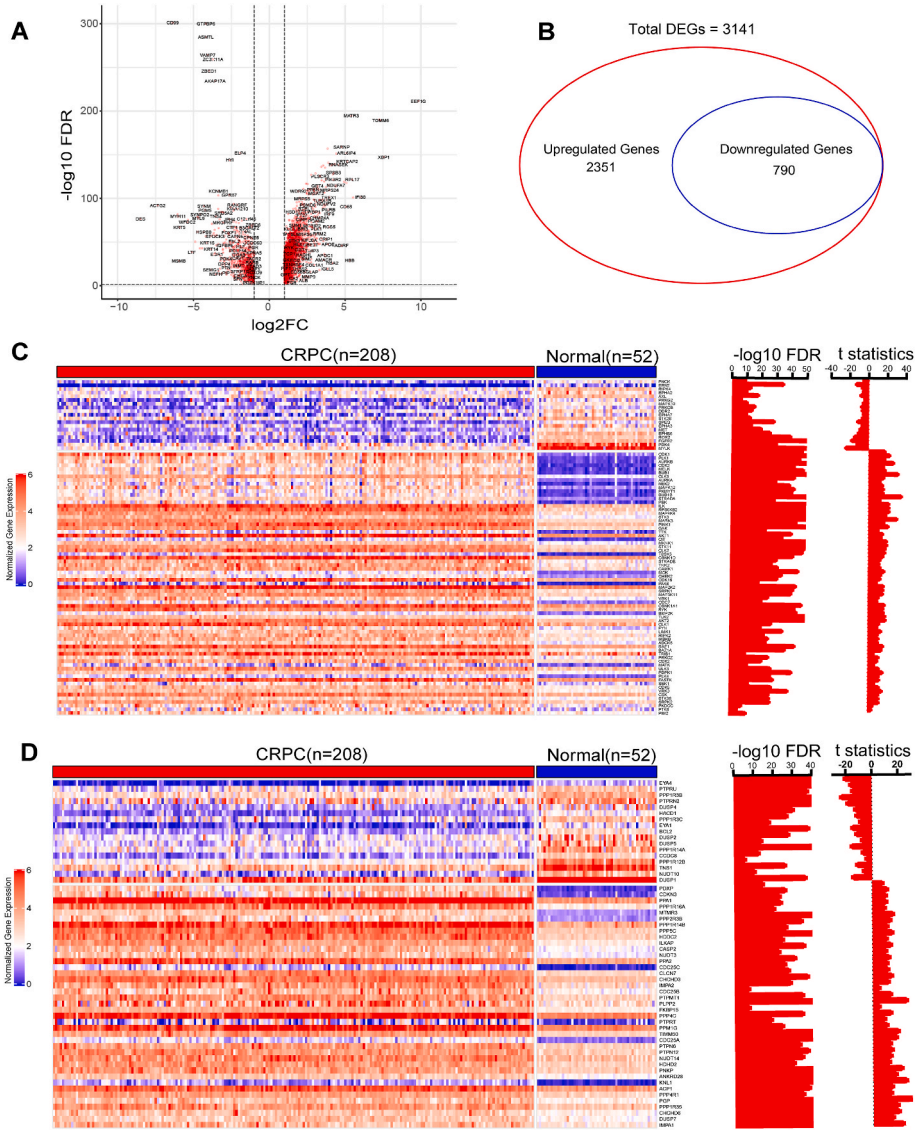

Fig. 1. Differential expression analysis of kinases and phosphatases

A. Volcano plot representing differentially regulated genes between CRPC patients (cbioportal, id: prad_su2c_2019, n = 208) and normal prostate (TCGA-GDC, id: TCGA-PRAD, n = 52), the left panel represents downregulated genes (log2FC < 1; FDR<0.01), and the right panel represents upregulated genes (log2FC > 1; FDR<0.01).

B. Venn diagram representing total number of differentially expressed genes along with up- and downregulated genes in CRPC patient samples.

C. Heatmap representation of patient level expression of differentially expressed kinases (prad_su2c_2019, n = 208 vs normal prostate, n = 52), with corresponding FDR and t-statistics plots, where upper section in the heatmap represents downregulated and lower section represents upregulated kinases (color red: high expression; blue: low expression).

D. Differential expression of phosphatases across CRPC patients (in prad_su2c_2019, n = 208 vs normal prostate, n = 52) represented in heatmap and corresponding FDR and t-statistics plots. Upper section in the heatmap represents downregulated phosphatases whereas lower section represents upregulated phosphatases (color red: High expression; blue: low expression).

2.8. Statistical analyses

We calculated the p-values of all the whiskers/box and bar plots by *t-test*. Log-Rank test, a standard statistical test used to calculate the statistical value of Kaplan-Meier survival estimates, was applied and generated the Log-rank p-values for all the survival plots. *False Discovery Rate (FDR)* and *t-statistics* for heatmaps were obtained from differential expression analysis pipeline *limma*.

3. Results

3.1. Differential expression analysis of kinases and phosphatase in CRPC patients

For DGE analysis, we obtained normal prostate expression data from TCGA-GDC (Study id: TCGA-PRAD, n = 52) and CRPC patient data from cbioportal (Study id: prad_su2c_2019, n = 208) respectively. Patient characteristics, pathological status of the tumour, resection/biopsy site and other details are summarized in Supplementary Tables 1 and 2 We performed DGE analysis using the limma pipeline, considering fold change >1.0 and false discovery rate (FDR) as <0.01 as significant. The expression analysis of 3141 genes revealed that 2351 genes (75 % of the total) were upregulated while 790 (25 % of the total) were downregulated (Fig. 1A, B and Supplementary Table 3) suggesting that upregulation of gene expression is a prominent pathological condition in CRPC. The dysregulated genes were scanned against the list of human kinases available at KinMap to identify the differentially expressed kinases in our list of genes. Heatmap analysis revealed that 90 human kinases were differentially expressed, amongst them; 71 were upregulated while 19 were downregulated compared normal prostate samples (Fig. 1C and Supplementary Table 4). We also analysed the expression profiles for phosphatases in the normal and CRPC samples. Total 57 phosphatases were found to be differentially expressed of which 40 were upregulated and 17 were downregulated in CRPC patients relative to normal individuals. Heat map showing the expression of phosphatases, with red and blue boxes representing the upregulated and downregulated phosphatases in each patient is summarized in Fig. 1D and Supplementary Table 5. Previous studies have shown that alterations in PI3K-Akt-mTOR pathway components occur in 100 % of the metastatic and 42 % of primary prostate tumors; thus, targeting the PI3K-Akt-mTOR pathway is considered a promising therapeutic approach for patients with CRPC [27]. It is also known that interplay between the PI3K/AKT and other signaling pathways, including the AR, WNT, and ERK signaling pathways, is crucial for disease progression and emergence of drug resistance in prostate cancer [28]. Interestingly, the highly dysregulated kinases and phosphatases identified in our analysis are associated with these pathways, suggesting the robustness of our analysis.

3.2. Differentially expressed kinases and phosphatases affect the overall survival of CRPC patients

Kaplan-Meier analysis is a powerful statistical method for estimating the survival of patients after encountering a disease or upon treatment. In our study, we employed Kaplan-Meier survival analysis to investigate the correlation between patient survival and expression levels of differentially expressed kinases and phosphatases. Analysis was performed by dividing the patients into two groups: group A consisted of patients with high expression of a kinase/phosphatase, and group B comprised patients with low expression of that particular kinase/phosphatase. We assessed the statistical significance of the estimates using a log-rank test. We hypothesized that for the upregulated kinases/phosphatases, candidates in group A must show a lower overall survival rate compared to group B. Conversely, for the downregulated kinases, group B must demonstrate a lower overall survival than group A, suggesting that a threshold level of these regulatory proteins is critical for disease manifestation. We performed survival analysis for the differentially expressed set of 90 kinases, keeping a high statistical significance (p-value <0.05). Our results demonstrated that 7 (CDK1, MARK3, MELK, PLK4, SRPK1, STK3, TTK) of the 71 upregulated kinases and 1 (SPEG) of the 19 down-regulated kinase were associated with lower overall survival (Fig. 2A and B). Similarly, survival analysis of the 57 differentially expressed phosphatases with the above mentioned criteria identified NUDT3, HDDC2, and PPA2 to be linked with decreased overall survival of CRPC patients (Fig. 2C). Collectively, our results suggest that variation in the expression of this subset of kinases and phosphatases is strongly associated with poor patient survival. Moreover, we also generated individual expression plots to analyse their expression levels and found them to be significantly dysregulated (Supplementary Fig. 1).

3.3. KPPS expression correlates with gleason score

The Gleason score (GS) is a tumor grading system used by pathologists to grade patient tumor biopsy samples to assess the similarity between normal and tumor cells, with GS6 representing the lowest and GS10 indicating the highest tumor grade score. Here, we performed expression analysis of KPPS in 167 CRPC patient tumor samples classified based on their Gleason score. We obtained patient data containing the Gleason score from cbioportal and extracted the samples with scores ranging from 6 to 10 (GS6, GS7, GS8, GS9, GS10) for further analysis. We found that while mRNA expression of KPPS is markedly higher in tumor samples across all Gleason scores compared to normal samples, a gradual increase in the mRNA expression is observed with increasing Gleason score for kinases MELK, PLK4, SRPK1 and phosphatase NUDT3. Conversely, the downregulated kinase SPEG exhibited consistent decrease in mRNA expression compared to normal samples across all Gleason score groups (Fig. 3A and B). The gradual increase in expression across different Gleason grade tumors suggests a potential association between these KPPS and relative aggressiveness of CRPC.

3.4. KPPS co-occur with top DEGs to promote tumorigenesis and are important for maintaining cellular fitness

Next, we investigated the co-occurrence of KPPS with the most probable oncogenes and tumor suppressor genes (with highest and lowest DEGs, respectively) identified in our expression analysis of 208 CRPC patients. For this, we considered genes with significant differential gene expression $|\log2FC > 3|$ for both up and downregulated candidates (top DEGs). Upon Reactome pathway enrichment analysis, candidates involved in growth and development were considered for the co-occurrence analysis with KPPS (Supplementary Table 6). We analysed the co-occurrence in prad_su2c_2019 data available on cbioportal. Employing a selection criteria of $|\text{p-value}<0.05|$, we identified 27 DEGs that significantly co-occurred with both kinases and phosphatases. Among the kinases, MELK, SRPK1, STK3, CDK1, and the phosphatase NUDT3 showed higher co-occurrence probability, while kinases such as PLK4, MARK3, TTK, and phosphatase PPA2 demonstrated lower co-occurrence probability with the top DEGs (Fig. 4a). Additionally, some kinases also frequently co-occur with each other, such as HDDC2 overlaps with TTK; NUDT3 overlaps with CDK1, MARK3, MELK, SRPK1, STK3, and PPA2 with PLK4, SRPK1, STK3, and TTK (Fig. 4A and Supplementary Table 7). We also observed strong co-occurrence between PLK4 and PPA2, MARK3 and MELK with NUDT3, and HDDC2 with TTK. (Fig. 4A and Supplementary Table 7).

Considering the noticeable outcome from our co-occurrence analysis, we further explored the efficiency of these KPPSs in prostate cancer cell lines. We obtained fitness dependency data of cancer cell lines from the DepMap portal (https://depmap.org/portal/) and extracted the fitness scores of KPPSs from 7 prostate cancer cell lines and one primary prostate epithelial cell line (Supplementary Table 8). This data, generated from three different large-scale RNAi screening datasets: Novartis Project DRIVE, Broad Institute Project Achilles, and Marcotte et al.

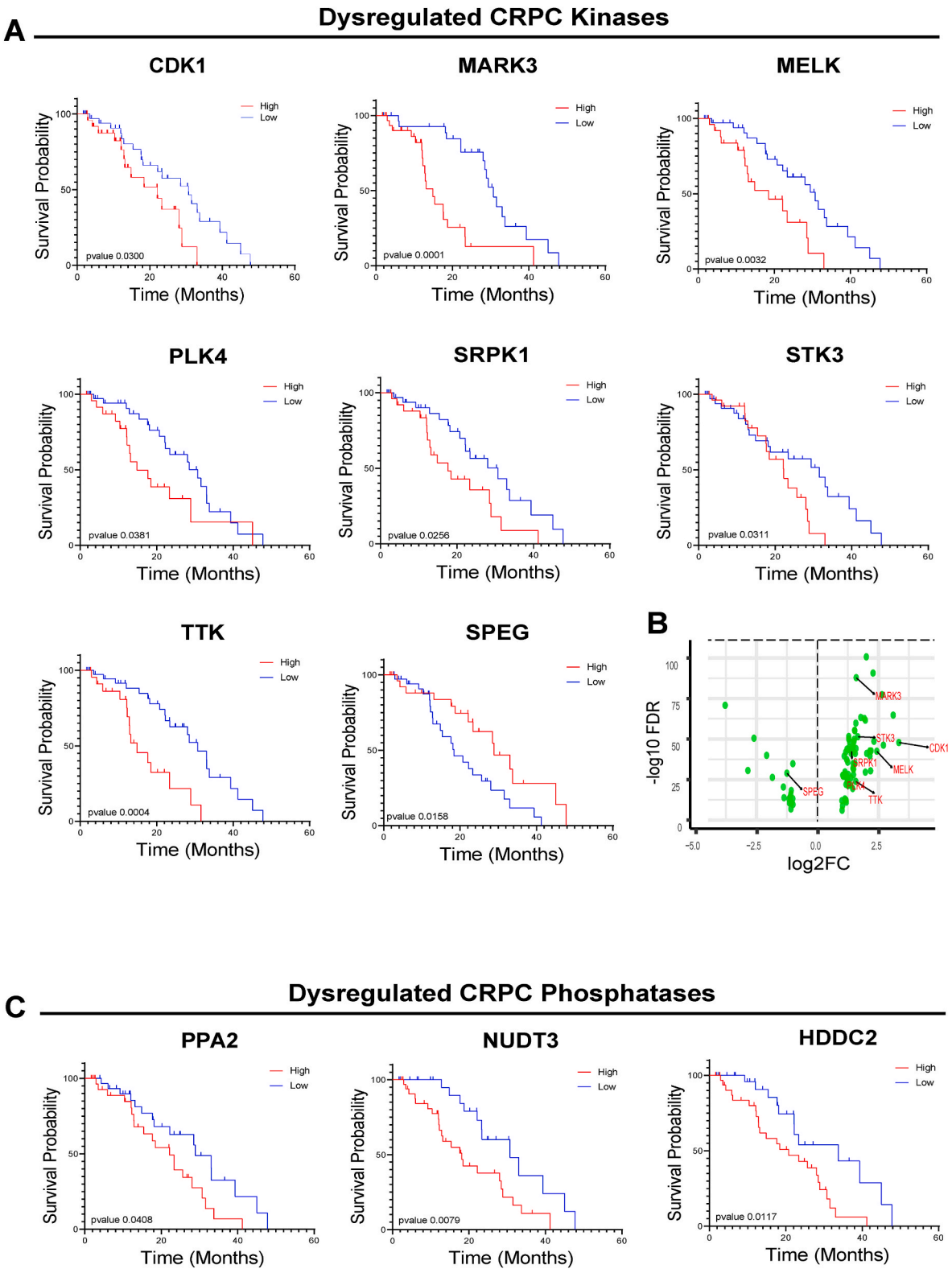

Fig. 2. Survival Analysis of CRPC patients

A. Kaplan-Meier survival estimates showing poor survival for patients with differentially expressed kinases (log-rank p-value cut off 0.05).

B. Volcano plot representation of differentially up and down-regulated kinases marked with significant kinases associated with poor survival outcome (left: downregulated kinases; right: upregulated kinases) (log2FC > 1; FDR<0.01) (marked genes: significant kinases).

C. Kaplan-Meier survival estimates showing poor survival for patients with differentially expressed phosphatases (log-rank p-value cut off 0.05).

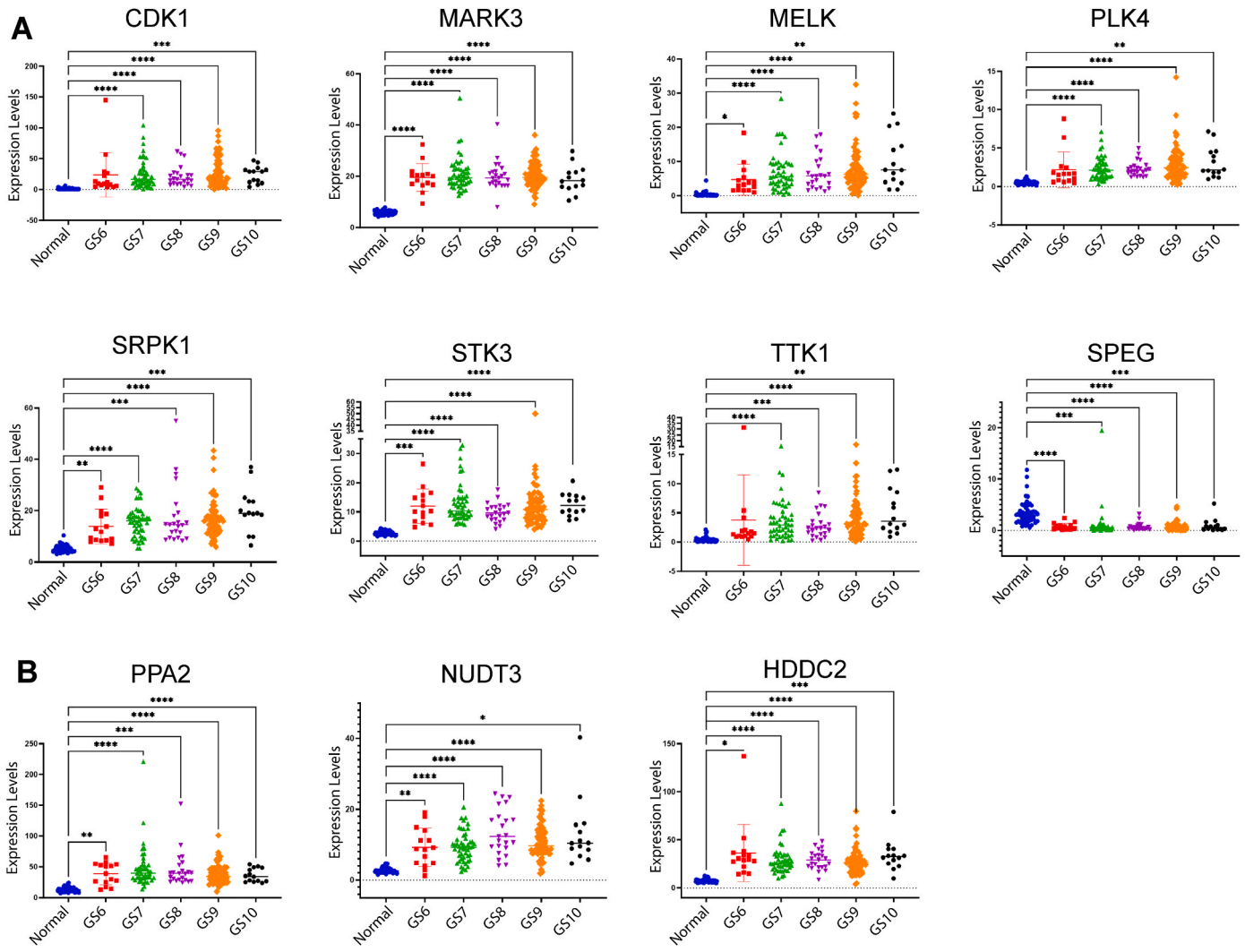

Fig. 3. mRNA expression of KPPS across the Gleason grade tumors represented as scatter plot (p-value: *0.05, **0.01, ***0.001, ****<0.0001).

dataset [29], allowed us to generate a heatmap to visualize the fitness dependency of each KPPS across the prostate cancer cell lines (Fig. 4B). Here, a negative score represents reduced fitness upon depletion of a particular gene, and it is vice versa in the case of a positive score. Loss of CDK1, known to mediate androgen receptor (AR) Ser-81 phosphorylation and increase AR protein expression, exhibited the most drastic decrease in the fitness of prostate cancer cell lines [30]. Loss of TTK, PLK4, and STK3 also strongly reduced fitness across all cell lines, while MARK3 and PPA2 moderately reduced fitness across multiple cell lines. Interestingly, loss of CDK1, TTK, PLK4, and MARK3 reduced the fitness of 22Rv1, a CRPC specific cell line.

To validate the accuracy and dependency of our analyses, we extracted expression data of 99 CRPC patients (TCGA-GDC, study id: WCDT-MCRPC) and 52 normal prostate samples (TCGA-GDC, study id: TCGA-PRAD), and considered them as secondary datasets. Patient characteristics, pathological status of the tumour, resection/biopsy site and other details are summarized in Supplementary Table 9. We performed similar analyses as in Fig. 1, and observed multiple common up and downregulated kinases between primary and secondary datasets (Supplementary Tables 10 and 11, Supplementary Fig. 1). The heatmap generated from the secondary dataset exhibited a strong resemblance with the primary dataset, validating the accuracy of our analyses. (Fig. 4C, Supplementary Fig. 4). Similar analyses was also performed for phosphatases, which also closely resembled the primary dataset (Fig. 4D) (Supplementary Table 11, Supplementary Fig. 2). Taken together, these analysis elucidate the co-occurrence patterns of KPPS with oncogenes and tumor suppressor genes in CRPC patients and assess the efficiency of these KPPSs in prostate cancer cell lines.

3.5. *MARK3 is an important player in CRPC progression*

Next, we explored the available literature to identify the role of KPPS in driving CRPC. Role of KPPS in various cancers including PCa and CRPC is summarized in Supplementary Table 12. Interestingly, our survey revealed that role of MARK3 in PCa/CRPC progression is still unknown. Earlier studies have shown that MARK3 is upregulated in human hepatocellular carcinoma and plays an oncogenic role via acting as a messenger in the WNT signaling pathway [31].

In this regard, first, we analysed MARK3 expression in CRPC samples (n = 99) & (n = 208) relative to primary prostate cancer (n = 498)and normal prostate samples (n = 52). Our results revealed that MARK3 expression is higher in CRPC samples compared to normal prostate samples (Supplementary Figs. 1 and 3).

Next, to elucidate the role of MARK3 in CRPC we performed cell viability and migration assays in two prostate cancer cell lines: 22Rv1 and PC3 upon MARK3 inhibitor (PCC0208017) treatment. PCC0208017 binds within the MARK3 active site and inhibits its kinase activity. It interacts with MARK3 through a combination of hydrophobic interactions, hydrogen bonding and salt bridge interactions. The pyrimidine moiety in PCC0208017 forms crucial hydrophobic interactions

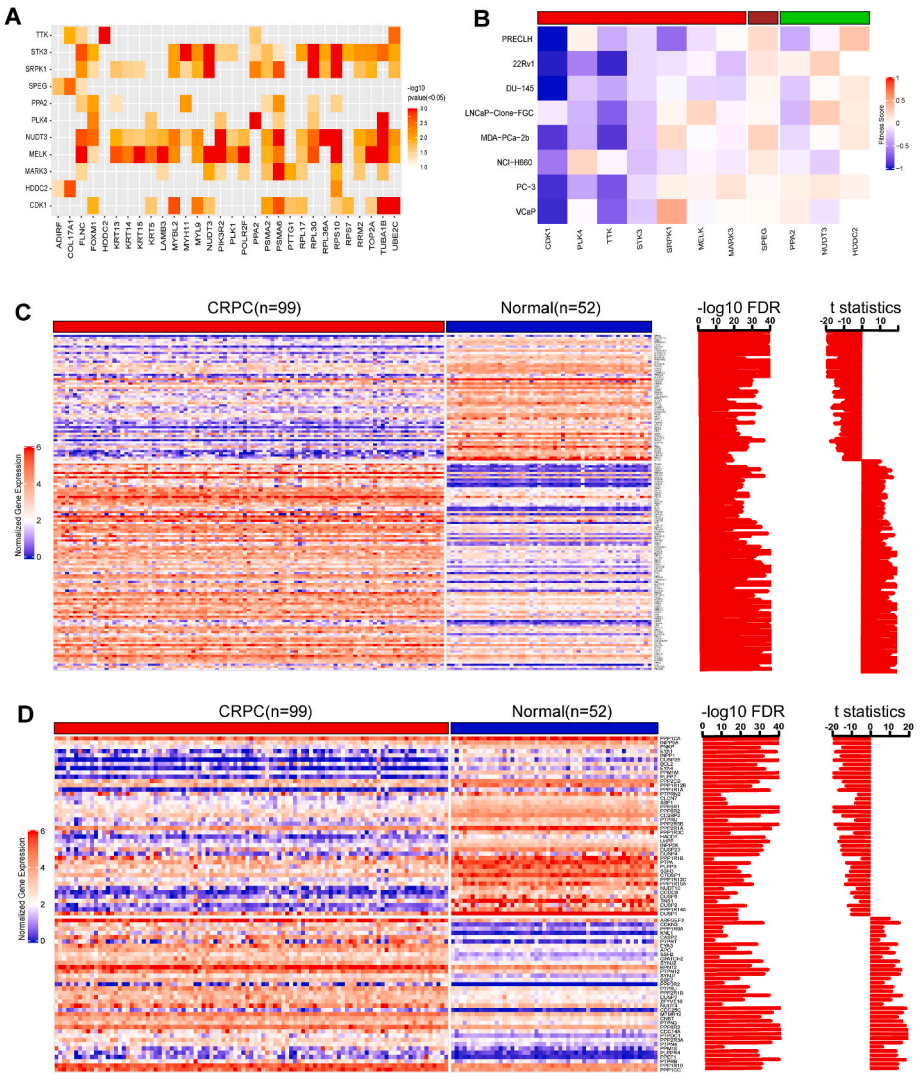

Fig. 4. Functional significance of KPPS and secondary validation

A. Co-occurrence of KPPS with top DEGs in CRPC patient data (prad_su2c_2019, n = 208 vs normal prostate, n = 52), where candidates on x-axis represent top DEGs and candidates on y-axis represents KPPS, and color intensity from yellow to red represents increasing -$\log_{10}$ values of p-values of each co-occurring event (selected co-occurrence events: p-value<0.05).

B. Fitness score of each KPPS across the prostate cancer cell lines (negative score: reduced fitness upon depletion of a gene; positive score: increased fitness upon depletion of a gene) (blue: reduced fitness; red: increased fitness).

C. Differential kinase expression in CRPC patients (TCGA-GDC, id: WCDT-MCRPC, n = 99) vs normal prostate samples (TCGA-GDC, id: TCGA-PRAD, n = 52) represented as heatmap, with corresponding FDR and t-statistics plots (color red: high expression; blue: low expression).

D. Differential phosphatase expression in CRPC patients (TCGA-GDC, id: WCDT-MCRPC, n = 99) vs normal prostate samples (TCGA-GDC, id: TCGA-PRAD, n = 52) represented as heatmap, with corresponding FDR and t-statistics plots (color red: high expression; blue: low expression).

with Val70, Met132, and Ala195, while nearby residues Ile62, Val116, Leu185, and Val205 also participate in establishing hydrophobic contacts. A hydrogen bond is formed between the secondary amine of PCC0208017 and Asp196 and the protonated piperidine ring's N-atom establishes a strong salt bridge with Glu139 and Asp142, enhancing its overall interaction strength with MARK3 [32].

22Rv1 is a cell line that possesses a castration-resistant phenotype and is commonly used in CRPC-specific studies. Upon treatment with MARK3 inhibitor, we observed that 22Rv1 is highly sensitive to PCC0208017 (Fig. 5A and B; Supplementary Fig. 4) with significant growth inhibition observed even at low concentrations (10 nM) and early time points (24 h). This effect was severe with time and higher concentration (Fig. 5A and B; Supplementary Fig. 4). IC50 values for each time point were 5.547 nM at 24 h (95 % CI: 3.168 to 9.715), 4.832 nM at 48 h (95 % CI: 2.836 to 8.199), and 3.614 nM at 72 h (95 % CI: 2.112 to 6.147). As a result, we conclude that the 22Rv1 cell line is highly sensitive to the MARK3 inhibitor PCC0208017. Next, we assessed the effect of MARK3 inhibition on the prostatic small cell neuroendocrine carcinoma cell line, PC3. It is an androgen-independent cell line that does not express androgen receptor (AR) and is used to study AR-independent pathways of prostate cancer progression. When PC3 cells were treated with PCC0208017, it was found that MARK3 inhibition resulted in slightly reduced cell growth and viability (Fig. 5C, D; Supplementary Fig. 5). However, the effect wasn't as significant as we observed on the 22Rv1 cell line. IC50 values for each time point were 148.3 nM at 24 h (95 % CI: 73.11 to 291.0), 6.697 nM at 48 h (95 % CI: 2.842 to 15.48), and 8.493 nM at 72 h (95 % CI: 4.360 to 17.28). These results suggest that differences in IC50 values of PCC0208017 in 22Rv1 and PC3 cells may be attributed to the differences in androgen receptor status (22Rv1 cells are AR-FL+/AR-V7+, while PC3 cells are AR-FL−/AR-V7−), growth characteristics, genetic profile, and metastatic potential. Taken together, these results indicate that MARK3 might be

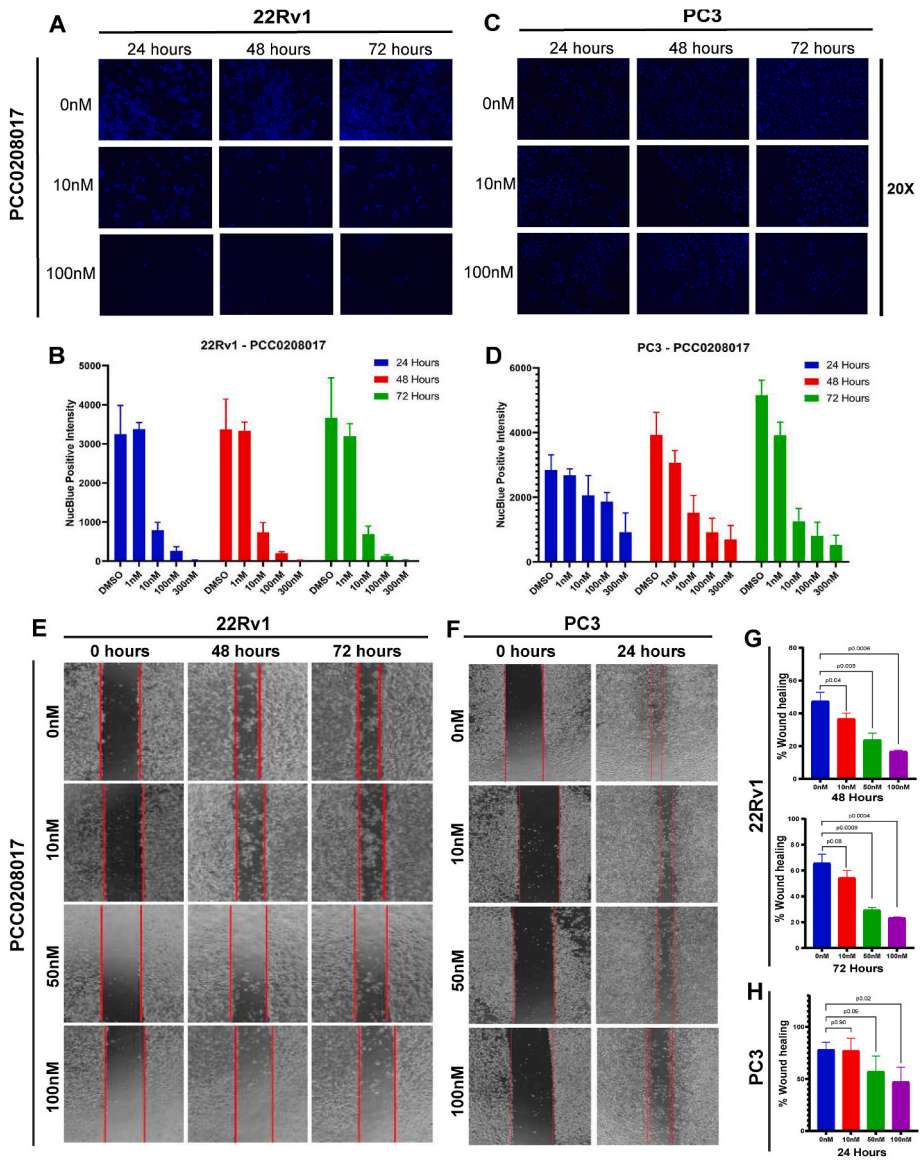

Fig. 5. Effect of MARK3 inhibition on CRPC and non-CRPC cell line

A. Representative images showing effect of PCC0208017 on the growth and viability of 22Rv1 cells 24, 48, and 72 h post-treatment with 0 nM, 10 nM, and 100 nM PCC0208017.

B. Bar plots representing the NucBlue intensity in 22Rv1 cells treated with varying concentrations of PCC0208017 at different time points.

C. Representative images showing effect of PCC0208017 on the growth and viability of PC3 cells 24, 48, and 72 h post-treatment with 0 nM, 10 nM, and 100 nM PCC0208017.

D. Bar plots representing the NucBlue intensity in PC3 cells treated with varying concentration of PCC0208017 at different time points.

E. Representative images showing the effect of PCC0208017 on migration potential of 22Rv1 cells treated with 0 nM, 10 nM, 50 nM, and 100 nM of PCC0208017.

F. Representative images showing the effect of PCC0208017 on migration potential of PC3 cells treated with 0 nM, 10 nM, 50 nM, and 100 nM of PCC0208017.

G. Bar plots representing the quantitation of migration potential of 22Rv1 cells treated with 0 nM, 10 nM, 50 nM, and 100 nM of PCC0208017.

H. Bar plots representing the quantitation of migration potential of PC3 cells treated with 0 nM, 10 nM, 50 nM, and 100 nM of PCC0208017.

related to the processes specifically driving CRPC progression.

Furthermore, we investigated the effect of MARK3 inhibition on cell migration using wound healing assay at multiple PCC0208017 concentrations. Consistent with the cell viability results, 22Rv1 cells exhibited significantly reduced migratory ability in response to increasing concentrations of PCC0208017 (0 nM, 10 nM, 50 nM, and 100 nM) (Fig. 5E–G) whereas the effect was less pronounced in PC3 cells (Fig. 5F–H). In conclusion, these results suggest that MARK3 may be crucial in driving CRPC progression, as evidenced by the heightened sensitivity of 22Rv1 cells to MARK3 inhibition and the associated reduction in migratory behavior.

3.6. *MARK3 inhibition induces cell cycle arrest*

Since MARK3 is known to be involved in the process of cell cycle progression, we performed flow cytometry-based cell cycle analysis in 22Rv1 and PC3 cells upon treatment with PCC0208017. The cells were treated with varying concentrations of PCC0208017 (0 nM, 10 nM, 50 nM, and 100 nM) for 24 h to assess its effect on different stages of cell cycle. Interestingly, we observe that cell cycle progression of 22Rv1 cells is drastically affected upon PCC0208017 treatment. Specifically, the treatment induces G1-phase arrest, accompanied by a reduction in the number of cells in the S- and G2/M-phases (Fig. 6A and B). Furthermore, while we observe minimal effect on cell cycle in PC3 cells, G2/M phase

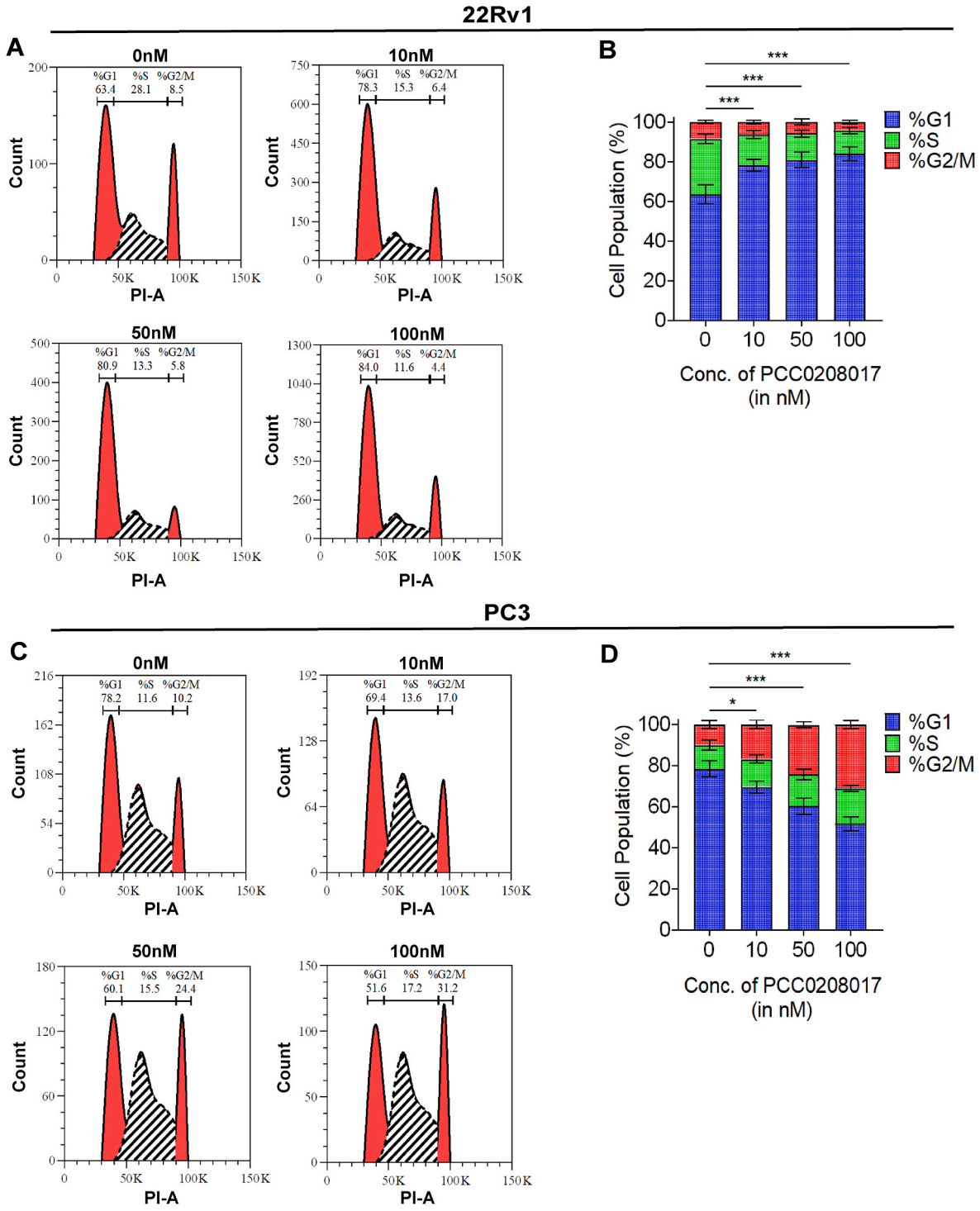

Fig. 6. MARK3 inhibition induces cell cycle arrest

A. Cell cycle analysis in 22Rv1 cells treated with DMSO or various concentrations of PCC0208017.

B. Bar plots representing the percentage of 22Rv1 cells in various phases of cell cycle upon treatment with DMSO or various concentration of PCC0208017. (p-value: ***0.001)

C. Cell cycle analysis in PC3 cells treated with DMSO or various concentrations of PCC0208017.

D. Bar plots representing the percentage of PC3 cells in various phases of cell cycle upon treatment with DMSO or various concentration of PCC0208017. (p-value: *0.05, ***0.001).

arrest is induced upon PCC0208017 treatment (Fig. 6C and D). These results suggest that MARK3 may play a role in the G1 phase of the cell cycle, particularly in 22Rv1 cells, which may be associated with the resistant phenotype in CRPC. Taken together, these results provide substantial evidence that MARK3 is a CRPC specific candidate that might be worthy of further exploration in CRPC therapeutics.

3.7. MARK3 inhibition downregulates genes involved in CRPC progression

In order to identify the molecular signatures affected upon MARK3 inhibition, we performed RNA sequencing in 22Rv1 cells upon DMSO or PCC0208017 treatment. DGE analysis identified that ~7933 genes were dysregulated post MARK3 inhibition (padj <0.05) (Fig. 7A; Supp. Table 13. Cancer hallmark analysis using gene set enrichment analysis (GSEA) tool detected a significantly negative enrichment of important PCa/CRPC gene sets involved in androgen response, epithelial-mesenchymal transition, mTORC1- and myc-signaling (Fig. 7 B). Notably, AR-V7 downstream target genes such as EDN2, ETS2, NPR3, UGT2B17, NUP210, and SLC3A2 were significantly downregulated, indicating that MARK3 affects AR-V7 mediated CRPC progression (Fig. 7C). Interestingly, our qRT-PCR analysis also demonstrated that MARK3 inhibition significantly affects the expression of other KPPS transcripts (Fig. 7D).

4. Discussion

Kinases and phosphatases are widely associated with cancer progression by post-translationally regulating protein function. Here, we have comprehensively analysed the gene expression and performed survival analysis of CRPC patient samples to identify candidate kinases and phosphatases associated with poor survival outcomes. Furthermore, we performed co-occurrence analysis of the KPPS with top differentially expressed genes in CRPC patients that are associated with cancer related processes. We found most of the KPPS were strongly co-occurring, pointing towards the functional relevance of KPPS in CRPC progression. Interestingly, the top DEGs significantly co-occur with KPPSs, and have a crucial role in driving CRPC. FOXM1, a master regulator in advanced prostate cancer, significantly co-occurs with KPPSs along with the MYBL2, RPS7, and RRM2, where transcription of FOXM1 is under the control of oncogenic transcription factors c-Myc and MYBL2. FOXM1 transcriptionally enhances RRM2 expression which inturn facilitates downstream MYC signalling resulting in CRPC progression. All the candidates associated with FOXM1-driven CRPC progression are known to provide ADT or docetaxel resistance in CRPC cells and enhance autophagy via the AMPK/mTOR pathway. Moreover, they also promote EMT transition and metastasis (Supplementary Table 14). Supplementary Table 1 lists the detailed description of top DEGs co-occurring with KPPS in PCa/CRPC progression. To assess their impact on cellular fitness, we explored the fitness dependency data for prostate cancer cell lines. We found that most of these candidates significantly affected cellular fitness upon their depletion, represented by the negative fitness score.

Our analyses identified numerous druggable kinases and phosphatases such as CDK1, STK3, MELK, PLK4, MARK3, TTK, SRPK1, SPEG, PPA2, NUDT3, and HDDC2. While some of these candidates such as CDK1, STK3, MELK, SRPK1, PLK4 and PPA2 have been previously studied for their role in PCa/CRPC development either computationally or experimentally [33], others such as SPEG, the only downregulated kinase shows promising impacts on fitness of prostate cancer cell lines upon depletion. However, it does not show a significant correlation with top DGEs, hence predicting its role in CRPC as a biomarker or novel target wasn't convincing. Further experimental testing will be required to check if ectopic expression of SPEG in prostate cancer cell lines affects their proliferation.

NUDT3 phosphatase is highly expressed in patient samples, affects their survival and co-occurs with most of the top DEGs. However, comprehensive studies will be required to pursue it as a drug target in CRPC, as reduced NUDT3 levels in breast cancer cells are known to

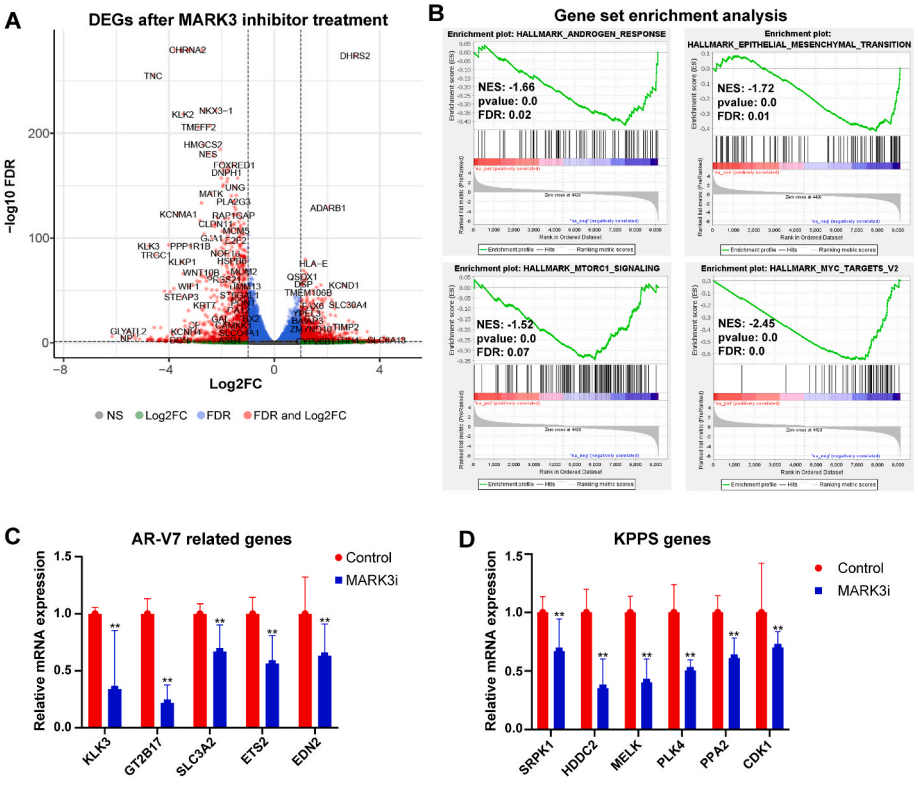

Fig. 7. RNA sequencing analysis in 22Rv1 cells upon MARK3 inhibition:
A. Volcano plot representing differentially expressed genes in 22Rv1 cells treated with DMSO or MARK3 inhibitor, PCC0208017.
B. GSEA plots showing enrichment of cancer hallmark gene sets; NES: Normalized Enrichment Score.
C. qRT-PCR analysis of AR-V7 target genes in cells treated with DMSO control or PCC0208017. (p-value: **0.01)
D. qRT-PCR analysis of KPPS genes in cells treated with DMSO control or PCC0208017. (p-value: **0.01).

promote cell migration in MCF-7 cells [34]. The role of HDDC2, an HD domain containing protein 2, is mostly unexplored in cancer or other human disease. It has been shown to be differentially expressed with a $|\log FC = 2.7|$ in the transcriptome sequencing study of nicotine-stressed normal breast epithelial cells [35]. In our analysis, we found that it is upregulated in CRPC patients and decreases the overall patient survival significantly. However its co-occurrence and fitness dependency analyses did not show promising results to pursue it as a drug target in CRPC.

Interestingly, MARK3 is a novel candidate among kinases that are unexplored for their role in PCa/CRPC progression. We found that inhibition of MARK3 with PCC0208017 significantly reduces cell viability and migration ability of both CRPC and non-CRPC cell lines. Additionally, its inhibition also induces G1-phase cell cycle arrest in 22Rv1 cells and G2/M-phase arrest in PC3 cells, suggesting its critical role in CRPC progression. Notably, MARK3 is upregulated in human hepatocellular carcinoma and plays an oncogenic role via acting as a messenger in the WNT signalling pathway [31]. CDC25C, a phosphatase that plays an important role in cell cycle regulation and promotes G2/M transition of mitotic cell by dephosphorylating CDK1 to activate cyclin B1/CDK1 complex, is a substrate of MARK3 [36–38]. Additionally AR-V7 expression has recently been shown to facilitate G2/M transition during CRPC progression [39]. These finding align with our observations that MARK3 inhibition induces G2/M arrest in PC3 cells, suggesting its role in promoting mitotic entry and tumorigenesis. Interestingly, MARK3 inhibition in 22Rv1 cells results in G1-phase arrest, suggesting that MARK3 might also be involved in the G1/S check point transition. IGF2BP2, a modulator of AR-V7 expression and drug resistance in CRPC cells regulates CDK6-mediated G1/S transition in breast cancer [40,41] suggesting a potential mechanistic link between MARK3 and resistance pathways in CRPC. Notably, FOXM1 and RRM2 contribute to CRPC drug resistance through the AMPK/mTOR pathway, facilitating S-phase entry. Our data shows a strong positive correlation between MARK3 and RRM2, however further experimental studies would be required to investigate the role of this correlation in G1-phase progression.

Our results also demonstrate that there is a steady increase in mRNA expression levels of the KPPS with increasing Gleason scores in prostate cancer patient samples. These findings suggest that these genes could be useful genetic indicators of tumor aggressiveness and may be able to complement the Gleason grading system in patient prognosis. However, further validation in larger patient cohorts would be required to confirm their clinical utility.

Overall, our findings demonstrate the role of MARK3 in regulating both G1/S and G2 cell cycle arrest, underscoring its importance in CRPC development and treatment resistance. While previous research has linked MARK3 to mitotic control, our findings expand its significance to treatment resistance mechanisms, providing a new perspective on how cell cycle dysregulation promotes CRPC progression. Furthermore, we show that KPPS (MELK, PLK4, SRPK1, TTK, NUDT3) can be used as molecular markers alongside Gleason grading. While various studies have investigated these genes in cancer pathways, such as MELK in cell cycle progression [42] and SRPK1 in splicing, our study is the first to link their expression to gradually increasing Gleason scores. This innovative integration could improve predictive accuracy by linking molecular biology and clinical utility to improve prostate cancer risk stratification and inform therapy choices.

Taken together, we expect that the results presented here will inspire further studies on testing the efficacy of MARK3 in clinical settings.

CRediT authorship contribution statement

Rajnikant Raut: Writing – review & editing, Writing – original draft, Visualization, Validation, Methodology, Investigation, Formal analysis, Data curation, Conceptualization. **Devesh Srivastava:** Writing – review & editing, Methodology, Formal analysis, Data curation. **Vinayak Nayak:** Writing – review & editing, Methodology, Formal analysis. **Taruna Saini:** Methodology, Formal analysis. **Parth Gupta:** Methodology, Formal analysis. **Amit Kumar Chakraborty:** Methodology. **Chumki Choudhury:** Methodology. **Manish V. Bais:** Resources. **Parul Mishra:** Writing – review & editing, Writing – original draft, Project administration, Funding acquisition, Conceptualization. **Ashish Misra:** Writing – review & editing, Writing – original draft, Supervision, Resources, Project administration, Investigation, Funding acquisition, Conceptualization.

Availability of data and materials

The gene expression data of CRPC patients used in this study are publicly available on genomic data commons data portal (GDC) [Healthy: TCGA-PRAD (https://portal.gdc.cancer.gov/projects/TCGA-PRAD); CRPC: WCDT-MCRPC (https://portal.gdc.cancer.gov/projects/WCDT-MCRPC)] and cBioportal [prad_su2c_2019 (https://www.cbioportal.org/study/summary?id=prad_su2c_2019)] of the cancer genome atlas (TCGA).

The raw RNA Sequencing data files for MARK3 inhibition have been deposited in GEO (GSE276660)

Ethical approval

None required.

Declaration of competing interest

None.

Acknowledgments

This work is supported by SERB (CRG/2022/008672) grant to A.M, HGK-IYBA (BT/11/IYBA/2018/08) and UoH-IoE-RC5-22-011 grants to P.M. R.R. duly acknowledges CSIR-SRF fellowship support. V.N., P.G. and T.S. are recipients of MoE-GoI fellowship. D.S. is a recipient of PMRF. P.M. acknowledges funding support from DBT BUILDER grant ((BT/INF/22/SP41176/2020).

Appendix A. Supplementary data

Supplementary data to this article can be found online at https://doi.org/10.1016/j.bbrep.2025.102003.

Data availability

Data will be made available on request.

References

[1] Y. Niu, C. Guo, S. Wen, J. Tian, J. Luo, K. Wang, H. Tian, S. Yeh, C. Chang, ADT with antiandrogens in prostate cancer induces adverse effect of increasing resistance, neuroendocrine differentiation and tumor metastasis, Cancer Lett. 439 (2018) 47–55, https://doi.org/10.1016/j.canlet.2018.09.020.

[2] J.-H. Lei, L.-R. Liu, Q. Wei, T.-R. Song, L. Yang, Y. Meng, P. Han, Androgen-deprivation therapy alone versus combined with radiation therapy or chemotherapy for nonlocalized prostate cancer: a systematic review and meta-analysis, Asian J. Androl. 18 (2016) 102–107, https://doi.org/10.4103/1008-682X.150840.

[3] T. Karantanos, P.G. Corn, T.C. Thompson, Prostate cancer progression after androgen deprivation therapy: mechanisms of castrate resistance and novel therapeutic approaches, Oncogene 32 (2013) 5501–5511, https://doi.org/10.1038/onc.2013.206.

[4] R.B. Marques, N.F. Dits, S. Erkens-Schulze, W.M. van Weerden, G. Jenster, Bypass mechanisms of the androgen receptor pathway in therapy-resistant prostate cancer cell models, PLoS One 5 (2010) e13500, https://doi.org/10.1371/journal.pone.0013500.

[5] N.D. Shore, R. Ionescu-Ittu, F. Laliberté, L. Yang, D. Lejeune, L. Yu, M.S. Duh, M. Mahendran, J. Kim, S.R. Ghate, Beyond frontline therapy with abiraterone and enzalutamide in metastatic castration-resistant prostate cancer: a real-world us study, Clin. Genitourin. Cancer 19 (2021) 480–490, https://doi.org/10.1016/j.clgc.2021.07.009.

[6] E. Francini, S. Yip, S. Ahmed, H. Li, L. Ardolino, C.P. Evan, M. Kaymakcalan, G. K. Shaw, P.W. Kantoff, M.-E. Taplin, N.S. Alimohamed, A.M. Joshua, D.Y.C. Heng, C.J. Sweeney, Clinical outcomes of first-line abiraterone acetate or enzalutamide for metastatic castration-resistant prostate cancer after androgen deprivation therapy + docetaxel or ADT alone for metastatic hormone-sensitive prostate cancer, Clin. Genitourin. Cancer 16 (2018) 130–134, https://doi.org/10.1016/j.clgc.2017.12.012.
[7] T.W. Flaig, R.C. Potluri, Y. Ng, M.B. Todd, M. Mehra, Treatment evolution for metastatic castration-resistant prostate cancer with recent introduction of novel agents: retrospective analysis of real-world data, Cancer Med. 5 (2016) 182–191, https://doi.org/10.1002/cam4.576.
[8] N.D. Shore, F. Laliberté, R. Ionescu-Ittu, L. Yang, M. Mahendran, D. Lejeune, L. H. Yu, J. Burgents, M.S. Duh, S.R. Ghate, Real-World treatment patterns and overall survival of patients with metastatic castration-resistant prostate cancer in the US prior to PARP inhibitors, Adv. Ther. 38 (2021) 4520–4540, https://doi.org/10.1007/s12325-021-01823-6.
[9] S.C. Baca, L.A. Garraway, The genomic landscape of prostate cancer, Front. Endocrinol. 3 (2012) 69, https://doi.org/10.3389/fendo.2012.00069.
[10] V. Kothari, J.F. Goodwin, S.G. Zhao, J.M. Drake, Y. Yin, S.L. Chang, J.R. Evans, K. Wilder-Romans, K. Gabbara, E. Dylgjeri, J. Chou, G. Sun, S.A. Tomlins, R. Mehra, K. Hege, E.H. Filvaroff, E.M. Schaeffer, R.J. Karnes, D.A. Quigley, D. E. Rathkopf, H.H. He, C. Speers, D.E. Spratt, L.A. Gilbert, A. Ashworth, A. M. Chinnaiyan, G.V. Raj, K.E. Knudsen, F.Y. Feng, DNA-dependent protein kinase drives prostate cancer progression through transcriptional regulation of the Wnt signaling pathway, Clin. Cancer Res. 25 (2019) 5608–5622, https://doi.org/10.1158/1078-0432.CCR-18-2387.
[11] C.M. Faltermeier, J.M. Drake, P.M. Clark, B.A. Smith, Y. Zong, C. Volpe, C. Mathis, C. Morrissey, B. Castor, J. Huang, O.N. Witte, Functional screen identifies kinases driving prostate cancer visceral and bone metastasis, Proc. Natl. Acad. Sci. U. S. A. 113 (2016) E172–E181, https://doi.org/10.1073/pnas.1521674112.
[12] Y. Cheng, L. Li, Z. Qin, X. Li, F. Qi, Identification of castration-resistant prostate cancer-related hub genes using weighted gene co-expression network analysis, J. Cell Mol. Med. 24 (2020) 8006–8017, https://doi.org/10.1111/jcmm.15432.
[13] R. Raut, P. Gupta, T. Saini, P. Mishra, A. Misra, Src kinase: an attractive therapeutic target for prostate cancer, in: Protein Kinase Inhibitors, Elsevier, 2022, pp. 479–503, https://doi.org/10.1016/B978-0-323-91287-7.00029-6.
[14] R. Ferraldeschi, D. Nava Rodrigues, R. Riisnaes, S. Miranda, I. Figueiredo, P. Rescigno, P. Ravi, C. Pezaro, A. Omlin, D. Lorente, Z. Zafeiriou, J. Mateo, A. Altavilla, S. Sideris, D. Bianchini, E. Grist, K. Thway, R. Perez Lopez, N. Tunariu, C. Parker, D. Dearnaley, A. Reid, G. Attard, J. de Bono, PTEN protein loss and clinical outcome from castration-resistant prostate cancer treated with abiraterone acetate, Eur. Urol. 67 (2015) 795–802, https://doi.org/10.1016/j.eururo.2014.10.027.
[15] K. McClinch, R.A. Avelar, D. Callejas, S. Izadmehr, D. Wiredja, A. Perl, J. Sangodkar, D.B. Kastrinsky, D. Schlatzer, M. Cooper, J. Kiselar, A. Stachnik, S. Yao, D. Hoon, D. McQuaid, N. Zaware, Y. Gong, D.L. Brautigan, S.R. Plymate, C. C.T. Sprenger, W.K. Oh, A.C. Levine, A. Kirschenbaum, J.P. Sfakianos, R. Sears, A. DiFeo, Y. Ioannou, M. Ohlmeyer, G. Narla, M.D. Galsky, Small-Molecule activators of protein phosphatase 2A for the treatment of castration-resistant prostate cancer, Cancer Res. 78 (2018) 2065–2080, https://doi.org/10.1158/0008-5472.CAN-17-0123.
[16] https://www.cbioportal.org, n.d.
[17] https://portal.gdc.cancer.gov, (n.d.).
[18] https://bioconductor.org/packages/release/bioc/html/TCGAbiolinks.html, (n.d.).
[19] https://rstudio.com/products/rstudio/download, (n.d.).
[20] http://www.kinhub.org/kinmap/, (n.d.).
[21] https://bioconductor.org/packages/release/bioc/html/EnhancedVolcano.html, (n.d.).
[22] https://www.bioconductor.org/packages/release/bioc/html/ComplexHeatmap.html, (n.d.).
[23] https://cran.r-project.org/web/packages/circlize/index.html, (n.d.).
[24] https://string-db.org, (n.d.).
[25] https://cran.r-project.org/web/packages/ggplot2/index.html, (n.d.).
[26] https://depmap.org/portal/, (n.d.).
[27] Y. Huang, X. Jiang, X. Liang, G. Jiang, Molecular and cellular mechanisms of castration resistant prostate cancer, Oncol. Lett. 15 (2018) 6063–6076, https://doi.org/10.3892/ol.2018.8123.
[28] Y. Yan, H. Huang, Interplay among PI3K/AKT, PTEN/FOXO and AR signaling in prostate cancer, Adv. Exp. Med. Biol. 1210 (2019) 319–331, https://doi.org/10.1007/978-3-030-32656-2_14.
[29] J.M. McFarland, Z.V. Ho, G. Kugener, J.M. Dempster, P.G. Montgomery, J. G. Bryan, J.M. Krill-Burger, T.M. Green, F. Vazquez, J.S. Boehm, T.R. Golub, W. C. Hahn, D.E. Root, A. Tsherniak, Improved estimation of cancer dependencies from large-scale RNAi screens using model-based normalization and data integration, Nat. Commun. 9 (2018) 4610, https://doi.org/10.1038/s41467-018-06916-5.
[30] S. Chen, Y. Xu, X. Yuan, G.J. Bubley, S.P. Balk, Androgen receptor phosphorylation and stabilization in prostate cancer by cyclin-dependent kinase 1, Proc. Natl. Acad. Sci. U. S. A. 103 (2006) 15969–15974, https://doi.org/10.1073/pnas.0604193103.
[31] T. Kato, S. Satoh, H. Okabe, O. Kitahara, K. Ono, C. Kihara, T. Tanaka, T. Tsunoda, Y. Yamaoka, Y. Nakamura, Y. Furukawa, Isolation of a novel human gene, MARKL1, homologous to MARK3 and its involvement in hepatocellular carcinogenesis, Neoplasia 3 (2001) 4–9, https://doi.org/10.1038/sj.neo.7900132.
[32] F. Li, Z. Liu, H. Sun, C. Li, W. Wang, L. Ye, C. Yan, J. Tian, H. Wang, PCC0208017, a novel small-molecule inhibitor of MARK3/MARK4, suppresses glioma progression in vitro and in vivo, Acta Pharm. Sin. B 10 (2020) 289–300, https://doi.org/10.1016/j.apsb.2019.09.004.
[33] C.K. Singh, R.A. Denu, M. Nihal, M. Shabbir, D.R. Garvey, W. Huang, K. A. Iczkowski, N. Ahmad, PLK4 is upregulated in prostate cancer and its inhibition reduces centrosome amplification and causes senescence, Prostate 82 (2022) 957–969, https://doi.org/10.1002/pros.24342.
[34] E. Grudzien-Nogalska, X. Jiao, M.-G. Song, R.P. Hart, M. Kiledjian, Nudt3 is an mRNA decapping enzyme that modulates cell migration, RNA 22 (2016) 773–781, https://doi.org/10.1261/rna.055699.115.
[35] J.H. Bavarva, H. Tae, R.E. Settlage, H.R. Garner, Characterizing the genetic basis for nicotine induced cancer development: a transcriptome sequencing study, PLoS One 8 (2013) e67252, https://doi.org/10.1371/journal.pone.0067252.
[36] K. Liu, M. Zheng, R. Lu, J. Du, Q. Zhao, Z. Li, Y. Li, S. Zhang, The role of CDC25C in cell cycle regulation and clinical cancer therapy: a systematic review, Cancer Cell Int. 20 (2020) 213, https://doi.org/10.1186/s12935-020-01304-w.
[37] P.V. Hornbeck, I. Chabra, J.M. Kornhauser, E. Skrzypek, B. Zhang, PhosphoSite: a bioinformatics resource dedicated to physiological protein phosphorylation, Proteomics 4 (2004) 1551–1561, https://doi.org/10.1002/pmic.200300772.
[38] P.V. Hornbeck, B. Zhang, B. Murray, J.M. Kornhauser, V. Latham, E. Skrzypek, PhosphoSitePlus, 2014: mutations, PTMs and recalibrations, Nucleic Acids Res. 43 (2015) D512–D520, https://doi.org/10.1093/nar/gku1267.
[39] T. Saini, P. Gupta, R. Raut, V. Nayak, P. Bharathnaveen, P. Mishra, A. Misra, AR-V7 expression facilitates accelerated G2/M phase transition in castration-resistant prostate cancer, Exp. Cell Res. 438 (2024) 114026, https://doi.org/10.1016/j.yexcr.2024.114026.
[40] T. Saini, D. Srivastava, R. Raut, P. Mishra, A. Misra, Insulin-like growth factor 2 mRNA -binding protein 2 (IGF2BP2) promotes castration-resistant prostate cancer progression by regulating AR - V7 mRNA stability, Cancer Reports 8 (2025) e70096, https://doi.org/10.1002/cnr2.70096.
[41] T. Xia, X. Dai, M. Sang, X. Zhang, F. Xu, J. Wu, L. Shi, J. Wei, Q. Ding, IGF2BP2 drives cell cycle progression in triple-negative breast cancer by recruiting EIF4A1 to promote the m6A-modified CDK6 translation initiation process, Adv. Sci. 11 (2024) 2305142, https://doi.org/10.1002/advs.202305142.
[42] Y. Goto, A. Kurozumi, T. Arai, N. Nohata, S. Kojima, A. Okato, M. Kato, K. Yamazaki, Y. Ishida, Y. Naya, T. Ichikawa, N. Seki, Impact of novel miR-145-3p regulatory networks on survival in patients with castration-resistant prostate cancer, Br. J. Cancer 117 (2017) 409–420, https://doi.org/10.1038/bjc.2017.191.